Electronic Supplementary Material (ESI) for Nanoscale.

Supporting Information

Boosting reversible oxygen electrocatalysis with enhanced interfacial pyridinic-N-Co bonding in cobalt oxide/mesoporous N-doped graphene hybrids

*Ting Feng, Xue-Ru Zhao, Cun-Ku Dong, Hui Liu, Xi-Wen Du, Jing Yang**

Institute of New-Energy Materials, Key Laboratory of Advanced Ceramics and Machining Technology of Ministry of Education, School of Materials Science and Engineering, Tianjin University, Tianjin 300072, China.

E-mail: yang_jing@tju.edu.cn

Experimental Section

1. Preparation Methods

Materials

All reagents were used in the experiments without further purification. Graphite powder was obtained from Sigma-Aldrich. Sulfuric acid (H_2SO_4), Potassium thiosulfate ($K_2S_2O_8$), Phosphorus pentoxide (P_2O_5), Acidic potassium permanganate ($KMnO_4$), Ethanol (CH_3CH_2OH) and hydrochloric acid (HCl) were bought from Tianjin Jiangtian Chemicals. 25% hydrogen peroxide (H_2O_2) and Zinc acetate were gained from Reagent Chemicals. Ammonia ($NH_3 \cdot H_2O$) was bought from Kermel. Cobalt chloride ($CoCl_2 \cdot 6H_2O$), Cobalt oxide (CoO) were obtained from Macklin. Nafion solution (5 wt%), KOH (99.98%), commercial Pt/C (20 wt%) and ruthenium oxide (RuO_2), were obtained from Tianjin Incole Union Technology Co., Ltd.

Synthesis of CoO, r-NLG, r-NG, CoO/r-NG and CoO/r-LG

The control sample of CoO was prepared with the same treatment but without NLG in pyrolysis treatments. Besides, the r-NLG and r-NG using NLG and NG as the precursor respectively, were prepared with the same treatment but without the $CoCl_2 \cdot 6H_2O$ in pyrolysis treatments. CoO/r-NG was prepared with the same treatment except that the NG sample was used to mixed up with $CoCl_2 \cdot 6H_2O$. The CoO/ r-LG was prepared with the same treatment except that the LGO sample was used to mixed up with $CoCl_2 \cdot 6H_2O$.

2. Materials Characterization

The powder X-ray diffraction (XRD) patterns of the samples were recorded on a Siemens-Bruker D5000 X-ray diffraction diffractometer with Cu K_α radiation. Transmission electron microscopy (TEM), high resolution TEM images (HRTEM), Energy dispersive spectrometer (EDS), EDS mapping were carried out on FEI Tecnai G2 F20 transmission electron microscope operated at 200 kV. X-ray photoelectron spectroscopy (XPS) analyses were performed using a PHI Quantum 2000 scanning ESCA Microprobe spectrometer. Infrared spectra of samples were recorded using a Bruker Tensor 27 FT-IR spectrometer in the range of 400-4000 cm^{-1}. The specific surface area of catalyst was evaluated by the Brunauer-Emmett-Teller (BET) method, which was carried out at -196 ˚C on Microporous instrument Tristar 3000. All samples were outgassed for 10 hours at 150˚C before measurements to remove any moisture or adsorbed contaminants that might be present on their surfaces.

3. Electrochemical Tests

Electrode Preparation

5 mg of the as-obtained catalyst were added to 970 μL of DI water, then 30 μL of Nafion solution (5 wt%) was added into the solutions. The mixture was ultrasonicated to achieve a well dispersed catalyst ink. Then, appropriate amount of the electrocatalyst ink were placed onto glassy carbon rotating disk electrode (RDE, 0.196 cm^2) or rotating ring disk electrode (RRDE, 0.247 cm^2) or carbon fiber paper (CFP, 0.1 cm^2) to keep a constant catalyst mass loading of 0.4 mg cm^{-2} for all the measurements except the Zinc-air battery test. For comparison, commercial Pt/C (20 wt%) and RuO_2 (99.95%) catalyst

inks were also prepared with the same method and mass loading.

Electrochemical Tests

Most electrochemical tests were performed on on a CHI 600E electrochemical workstation, except that ORR related tests were obtained on a wave drive 20 workstation (Pine Research Instruments, US). All tests were used a three-electrode system including a platinum foil counter electrode, a saturated calomel reference electrode, and a working electrode. The reference electrode was calibrated in H_2-saturated 0.1 and 1 M KOH solution before measurements. For ORR, catalysts were placed on RDE or RRDE as the working electrode. For OER, catalysts were loaded on CFP, and tested in 1 M KOH solutions with O_2 saturated. All the linear sweep voltammograms (LSV) were measured at a scan rate of 5 mV s^{-1}. Additionally, the ORR polarization curves were corrected by subtracting the background current for Nitrogen-saturated electrolyte.

The Koutechy-Levich (K-L) equations (1)–(3) were used to calculate the kinetic current density (J_k) and transferred electron numbers (n). The Koutechy-Levich (K-L) equations (1)–(2) are used to calculate the kinetic current density (J_k) and transferred electron numbers (n).

$$\frac{1}{J} = \frac{1}{J_d} + \frac{1}{J_k} = \frac{1}{B\omega^{1/2}} + \frac{1}{J_k} \quad (1)$$

$$\omega = 0.2nFD_0^{2/3}\nu^{-\frac{1}{6}}C_0 \quad (2)$$

Where J, J_d, and J_k, represent the measured, diffusion-limiting, and kinetic current density,

respectively. Where n is the electron transfer number, F the Faraday constant (96485 C mol^{-1}), A the electrode area (cm^2), C_0 the saturated O_2 concentration (1.21×10^{-6} mol cm^{-3}), D the diffusion coefficient of the dissolved O_2 (1.86×10^{-5} cm^2 s^{-1}), and υ the kinetic viscosity of solvent (0.01 cm^2 s^{-1}). ω stands for the rotation rate of RDE in unit of rpm. What's more, to calculate the percentage of peroxide produced during ORR ($H_2O_2\%$) and transferred electron numbers (n) with different calculation methods, RRDE was used. J_D is the disk current and J_R is the ring current and both of them are got by RRDE.

$$n = \frac{4J_D}{J_D + (\frac{J_R}{N})} \quad (3)$$

$$H_2O_2\% = 100\frac{2(\frac{J_R}{N})}{J_D + J_R/N} \quad (4)$$

EIS was tested at a potential of 1.55 V vs. RHE and in a frequency range from 0.1 to 10^6 Hz. The electrochemical double-layer capacitance (C_{dl}) was obtained by performing CV measurements at different scan rates of 5, 10, 15, 20, and 25 mV s^{-1}. A plot of the charging current density (Jc) at 1.15 V vs. RHE, against the scan rates gives a straight line with a slope equal to C_{dl}. Then the ECSA could be calculated based on Equation (5).

$$ECSA = \frac{C_{dl}}{C_s} \quad (5)$$

where C_s is the specific capacitance of the sample or the capacitance of an atomically smooth planar surface with unit area under identical electrolyte conditions.

Zn-Air Battery Assembly

The Zn-air battery was consists of a zinc plate as the anode, CoO/r-NLG or a mixture of Pt/C and RuO_2 loaded on carbon paper (0.8 mg cm^{-2}) as the air cathode, and a solution of 6.0 M KOH and 0.2 M $Zn(Ac)_2$ as the electrolyte. The battery performance was measured by CHI 600E electrochemistry workstation. The oxygen flow towards the air cathode was maintained during the measurements.

Supplementary Figures

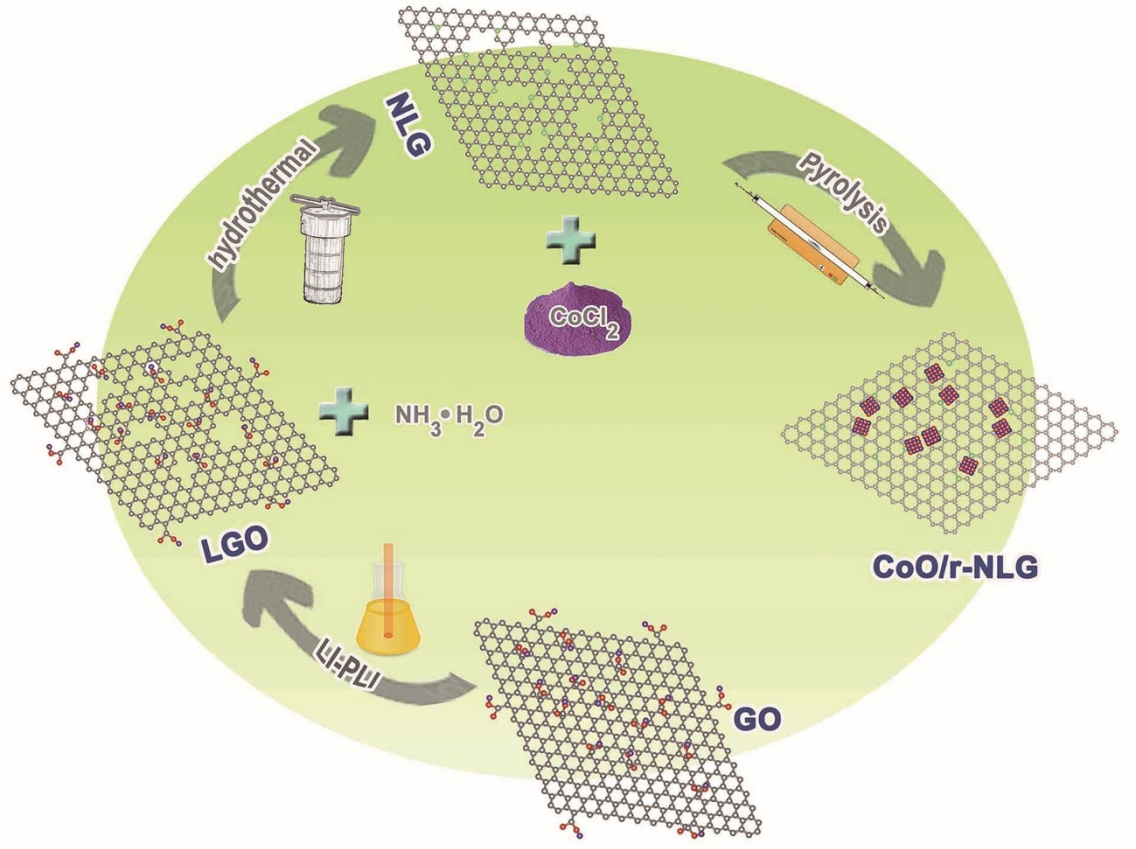

Figure S1. Schematic illustration of the preparation of CoO/r-NLG hybrid for reversible oxygen electrocatalysis.

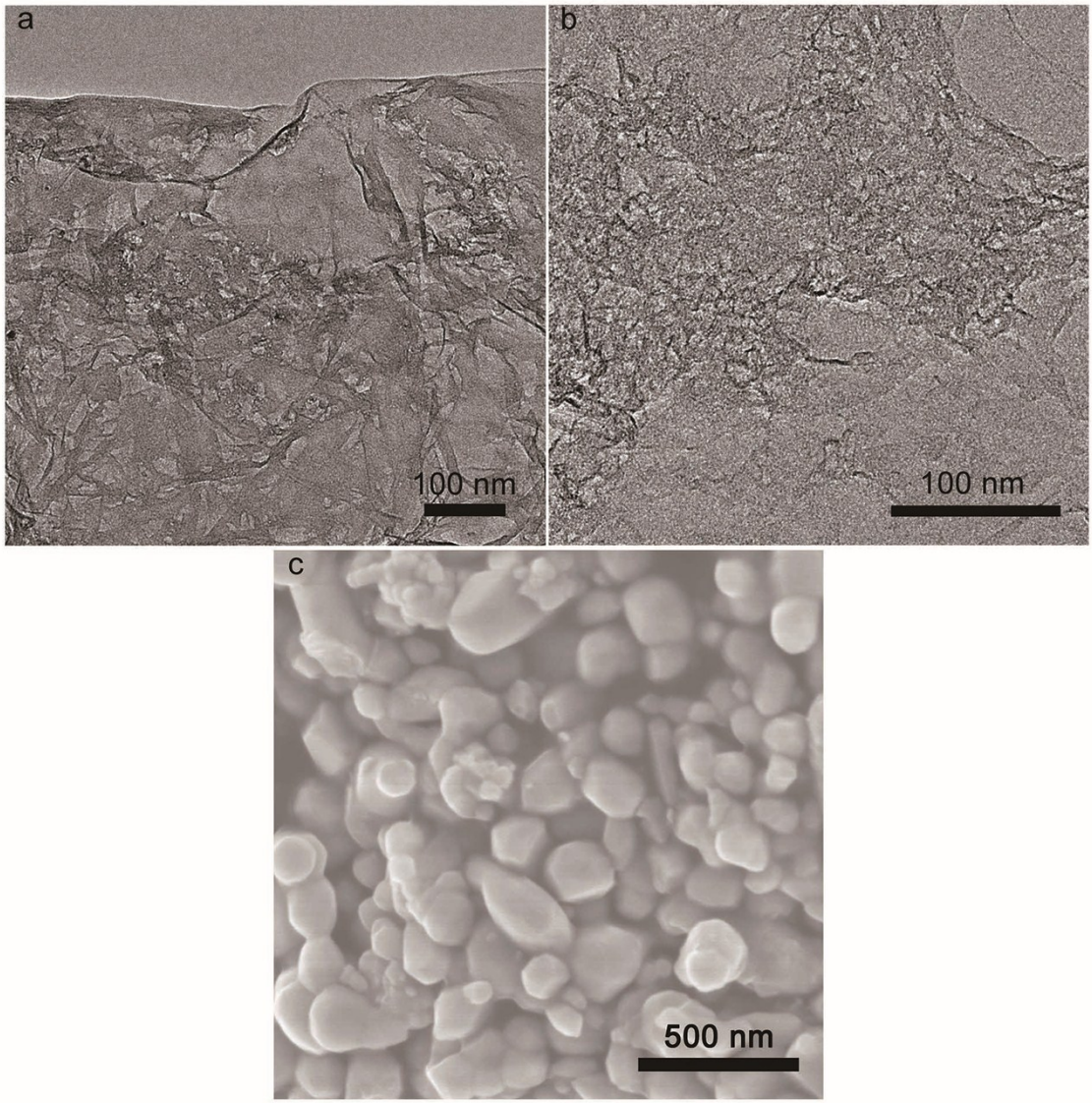

Figure S2. (a) TEM of NLG; (b) TEM of r-NLG; (c) SEM of CoO.

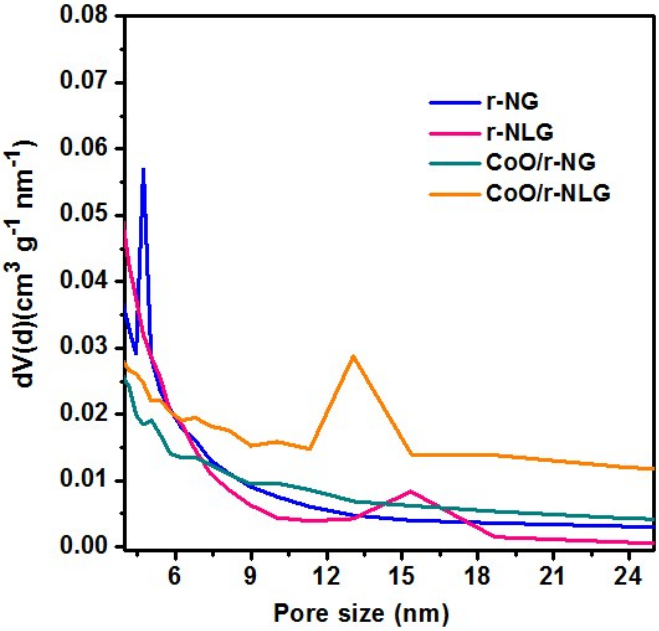

Figure S3. Pore size distribution of r-NG, r-NLG, CoO/r-NG, and CoO/r-NLG.

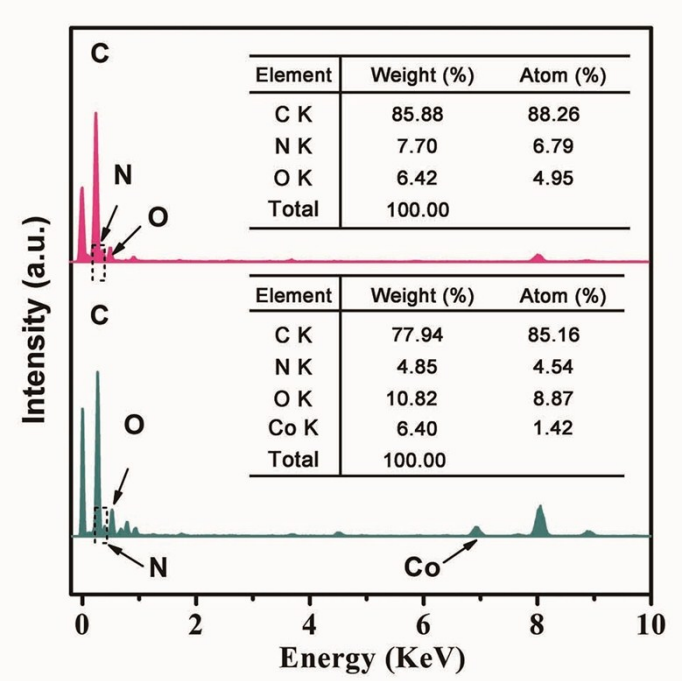

Figure S4. EDS of r-NLG and CoO/r-NLG.

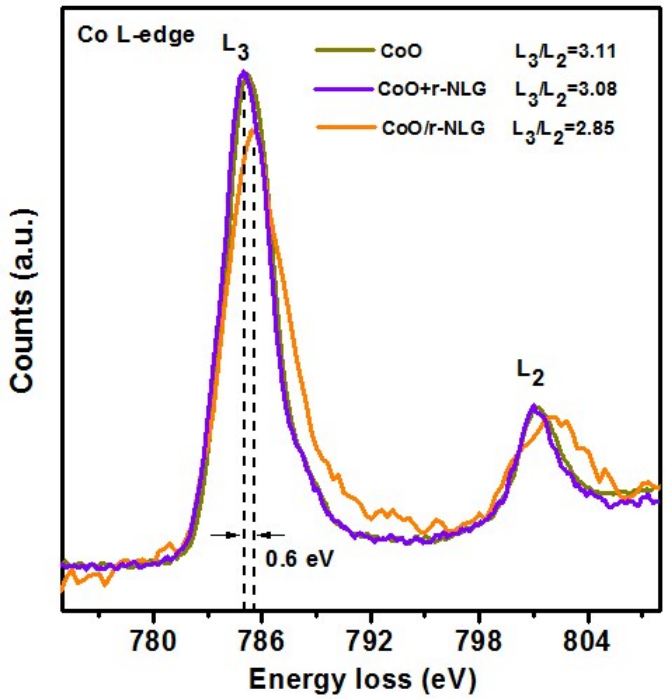

Figure S5. Cobalt L-edge EELS spectra of CoO/r-NLG, CoO+r-NLG, and CoO NPs.

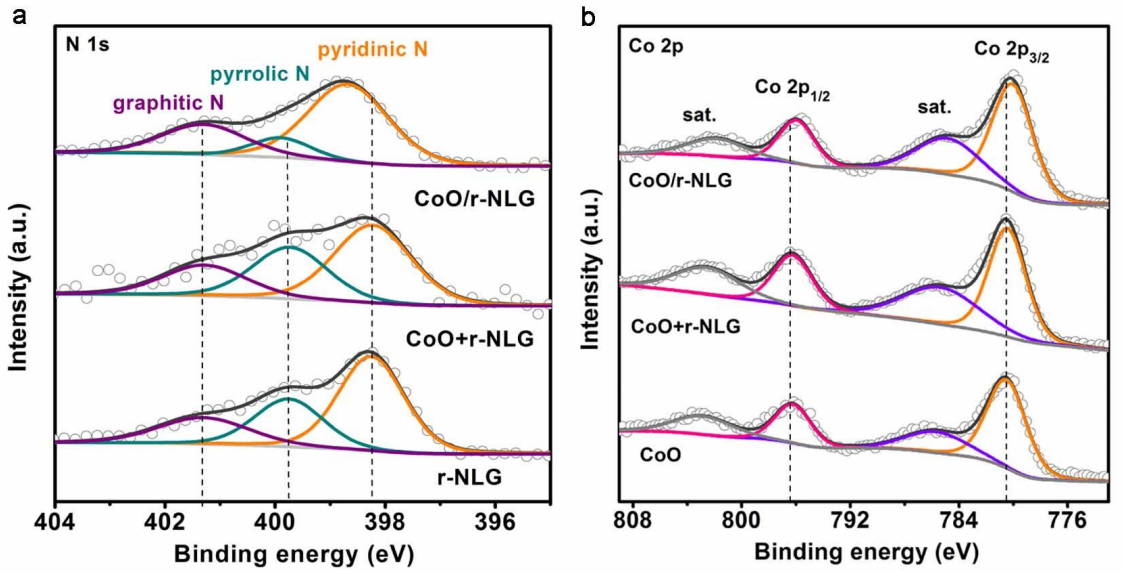

Figure S6. (a) High-resolution XPS N 1s spectra of CoO/r-NLG, r-NLG, and CoO + r-NLG. (b) Co 2p spectra of CoO/r-NLG, CoO + r-NLG, and CoO NPs.

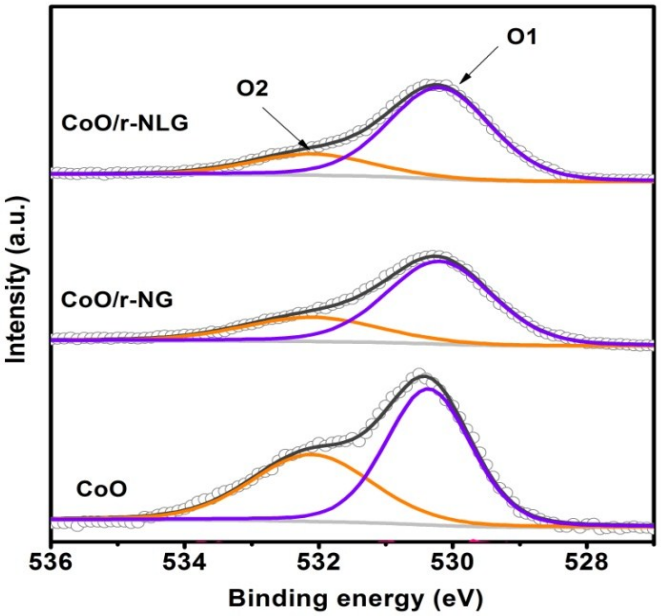

Figure S7. High resolution XPS O 1s spectra of CoO/r-NLG, CoO /r-NG, and CoO.

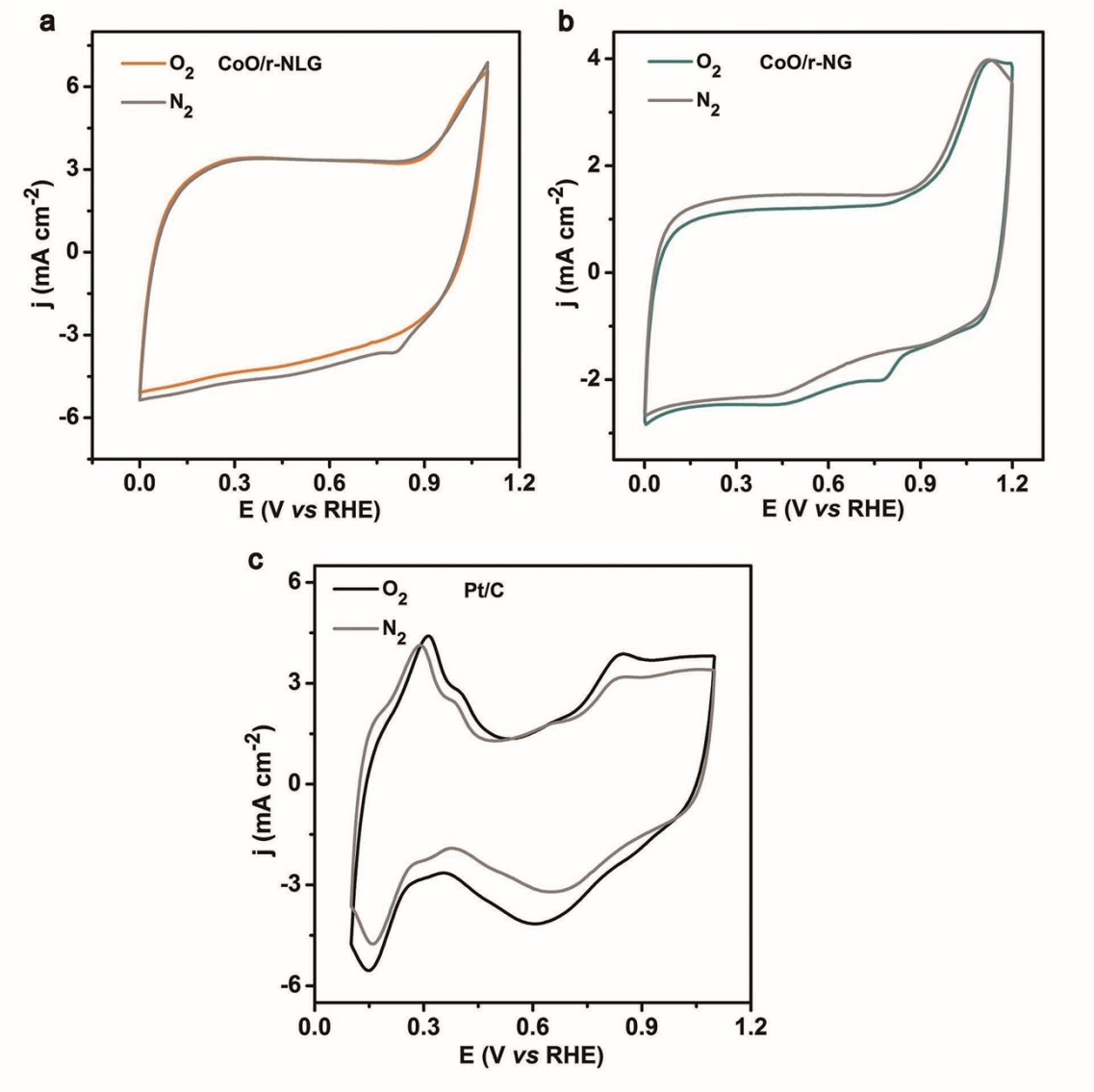

Figure S8. CV curves of some samples in O_2 saturated and N_2 saturated 0.1 M KOH solution, (a) CoO/ r-NLG, (b) CoO/ r-NG, (c) Pt/C.

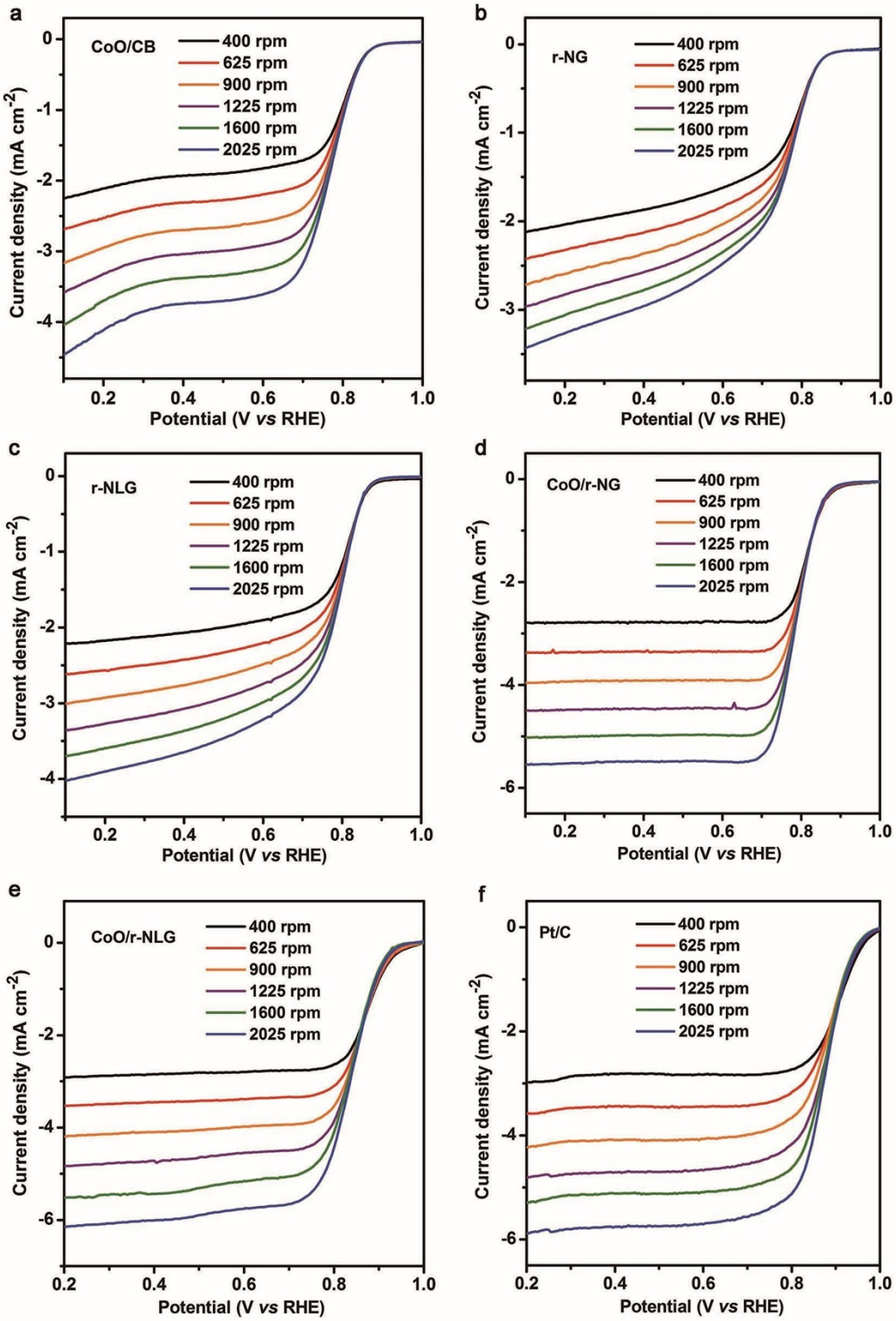

Figure S9. ORR LSV curves for (a) CoO/CB, (b) r-NG, (c) r- NLG, (d) CoO/ r-NG, (e) CoO/ r-NLG, and (f) Pt/C measured in 0.1 M KOH.

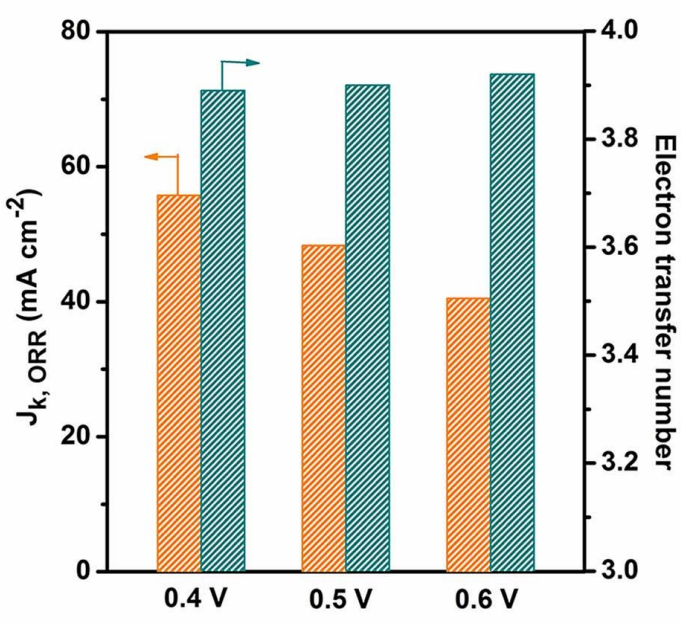

Figure S10. The kinetic currents j_k and electron transfer number for CoO/r-NLG at potentials of 0.4 V, 0.5 V, and 0.6 V, which were calculated based on the K−L equation.

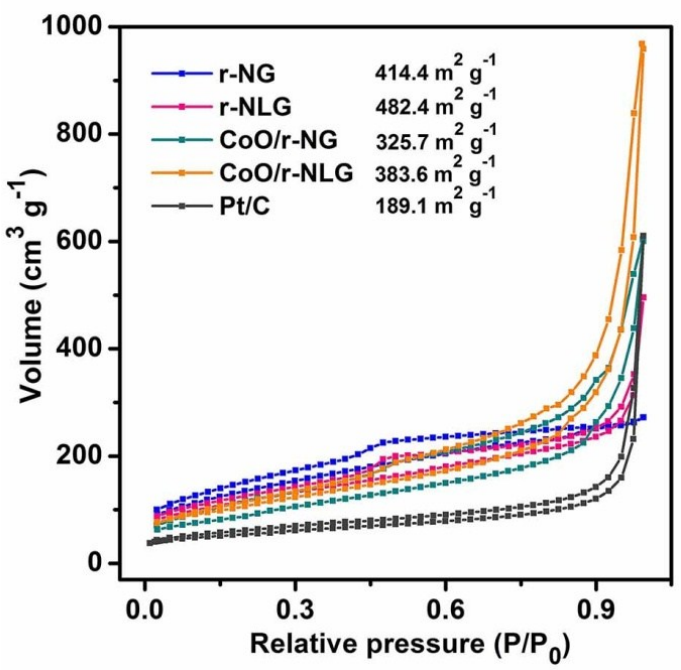

Figure S11. N_2 adsorption/desorption isotherm of r-NG, r-NLG, CoO/ r-NG, CoO/ r-NLG, and Pt/C.

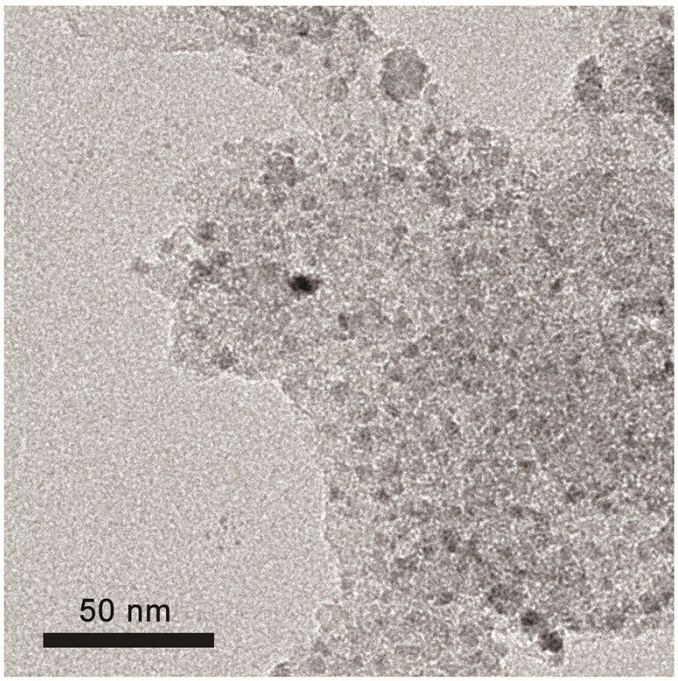

Figure S12. TEM images of CoO/r-NLG after 12 h ORR test.

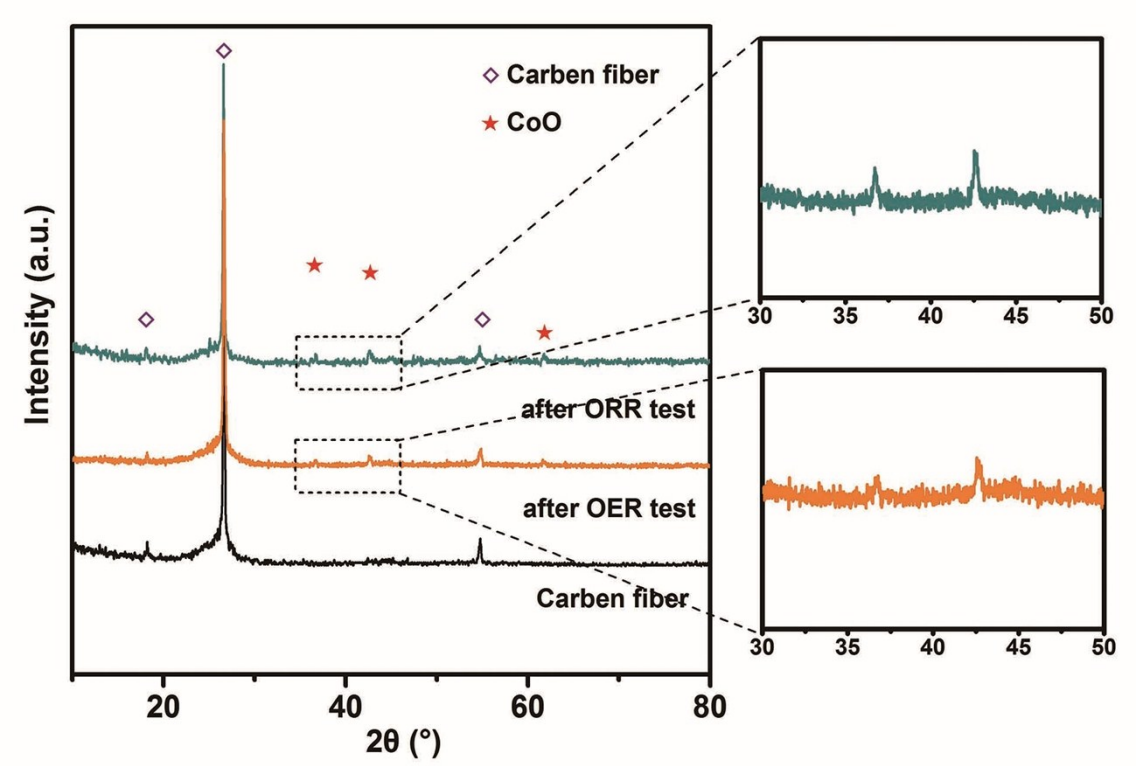

Figure S13. XRD pattern of CoO/r-NLG after 12 h ORR and OER tests, respectively.

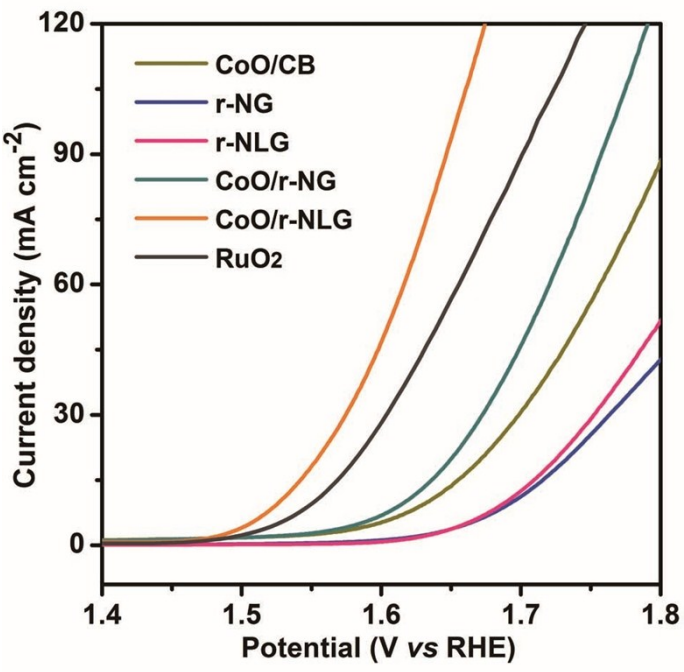

Figure S14. The OER polarization curves without *iR* correction in O_2-saturated 1.0 M KOH.

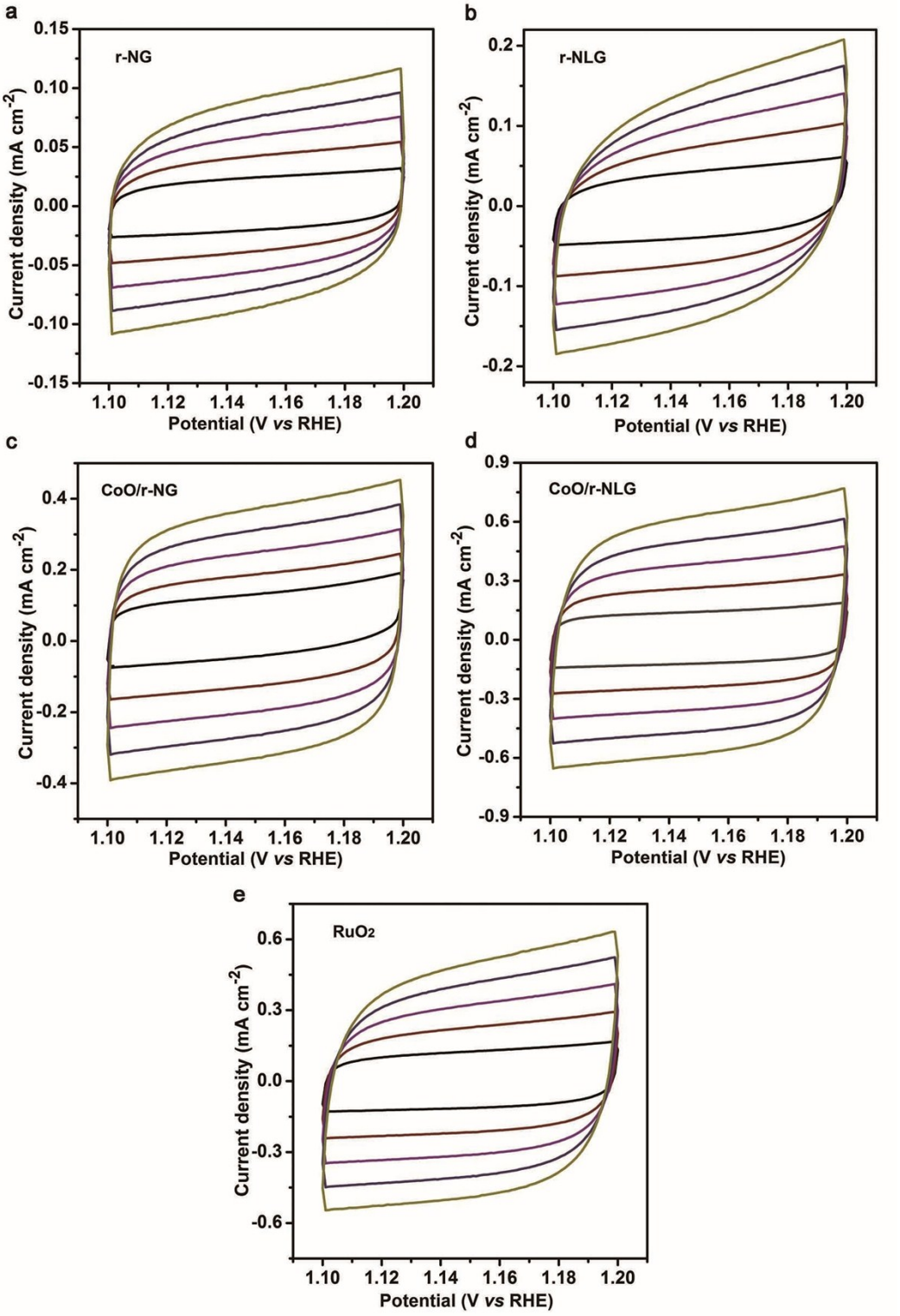

Figure S15. (a-e) CV curves obtained in a potential window of 1.10-1.20 V vs. RHE at different scan rates in 1.0 M KOH for r-NG, r-NLG, CoO/r-NG, CoO/r-NLG, and RuO_2, respectively.

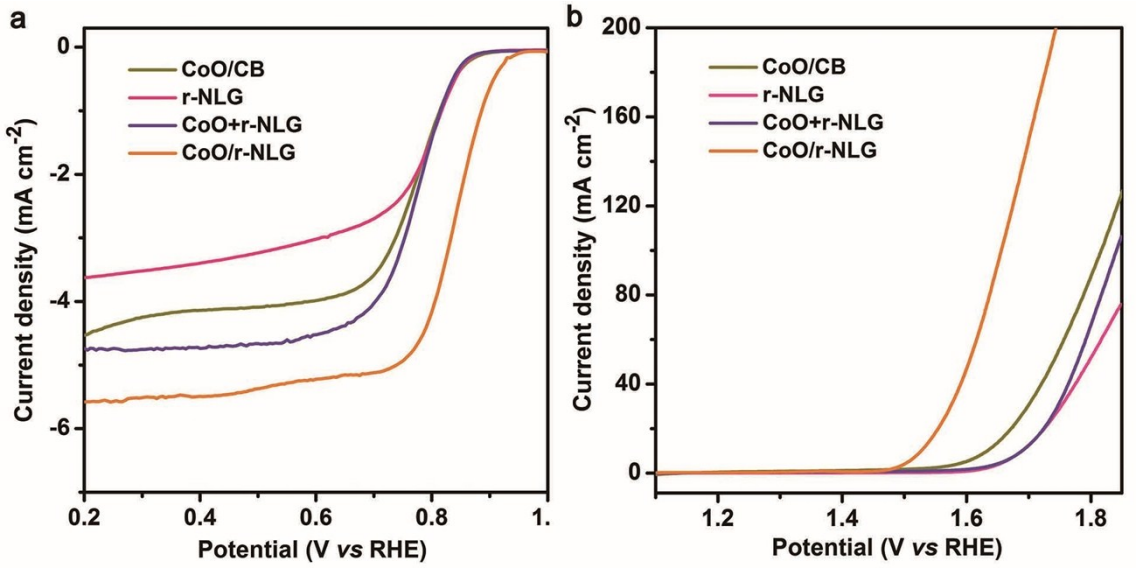

Figure S16. ORR (a) and OER (b) LSV curves for CoO/CB, r-NLG, CoO+ r-NLG, and CoO/r-NLG.

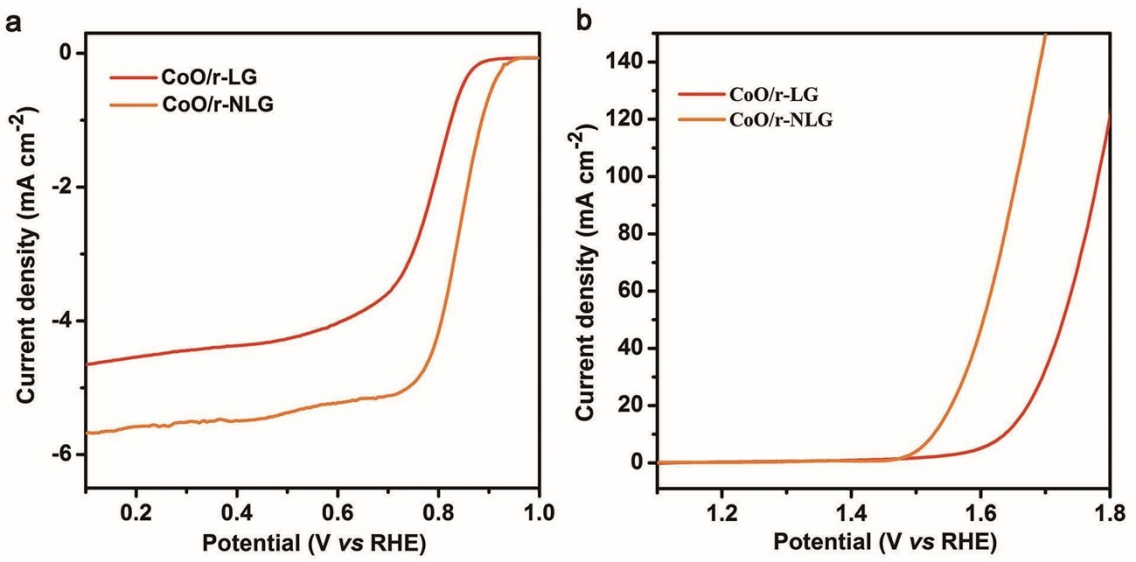

Figure S17. ORR (a) and OER (b) LSV curves for CoO/r-LG and CoO/r-NLG.

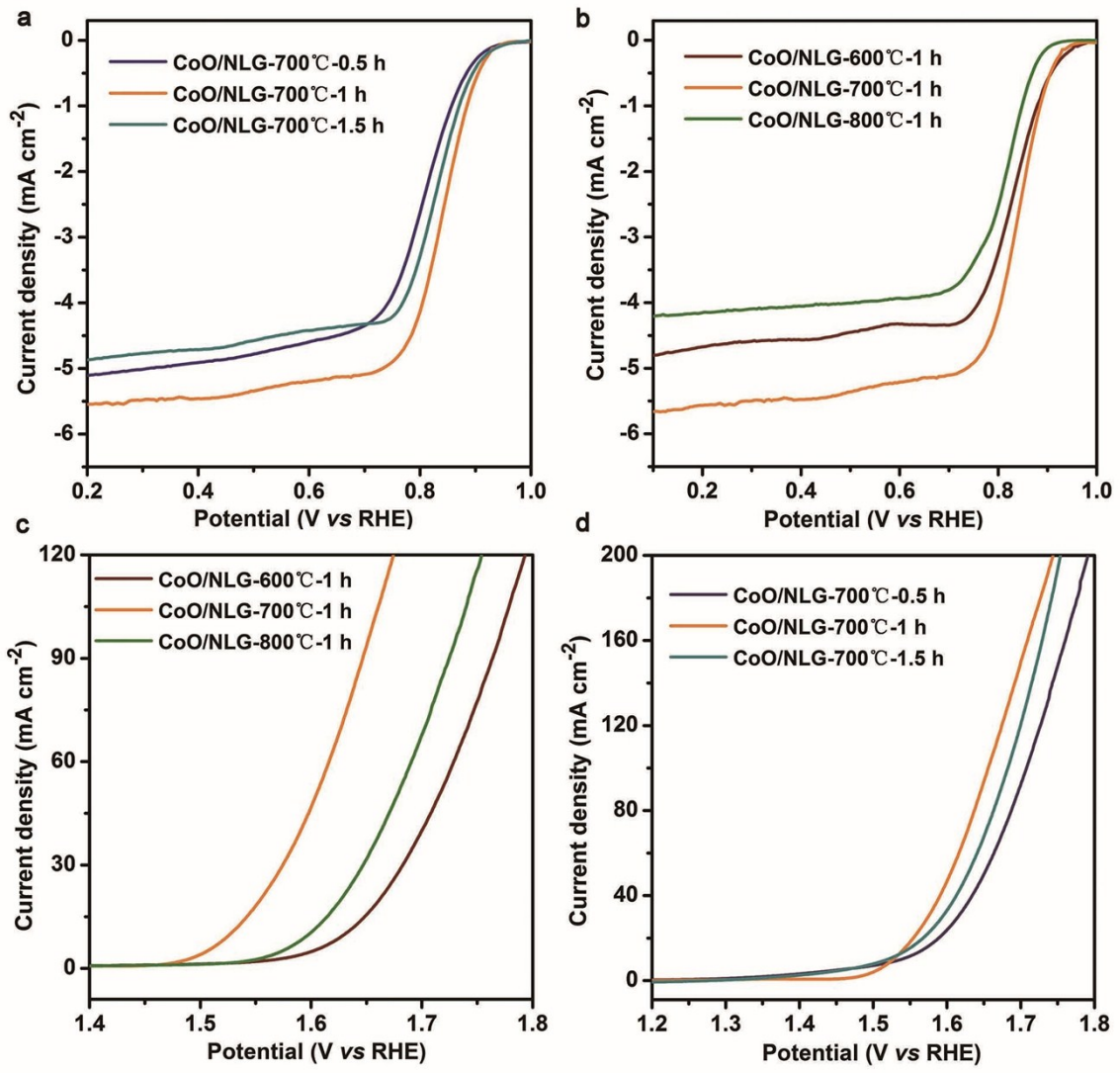

Figure S18. ORR (a,b) and OER (c,d) LSV curves for the as-obtained catalyst prepared at different heating temperatures and time.

Supplementary Tables

Table S1. Nitrogen contents in the nitrogen-doped samples.

Catalyst	Total N (at%)	Pyridinic N (at%)	Pyrrolic N (at%)	Graphitic N (at%)
r-NG	4.24	1.72	1.68	0.84
r-NLG	6.83	3.55	1.97	1.31
CoO/r-NG	4.68	2.19	1.42	1.07
CoO/r-NLG	7.49	4.7	0.98	1.81

Table S2. Weight percentages of Co ions and CoO in the hybrid samples.

Catalyst	Co (wt%)	CoO (wt%)
CoO/r-NG	13.64	17.34
CoO/r-NLG	14.87	18.91

Table S3. Comparison of the oxygen electrode activities of the recently reported highly active ORR/OER bi-functional catalysts. $E_{j=10}$ is the operating potentials to deliver a 10 mA cm^{-2} current density for OER. $E_{1/2}$ is the ORR half-wave potential. $\Delta E = E_{j=10} - E_{1/2}$ is a measure of the overall oxygen electrode activity.

Catalyst	Electrolyte	Catalyst loading (mg cm^{-2})	$E_{j=10}$ (V vs. RHE)	$E_{1/2}$ (V vs. RHE)	ΔE (V)	Ref.
N-GRW	0.1M KOH	0.6	1.59	0.84	0.75	[1]
P,S-CNS	0.1M KOH	0.15	1.59	0.87	0.72	[2]
Co_3O_4/NPGC	0.1M KOH	0.2	1.68	0.84	0.84	[3]
Co-N-CNTs	0.1M KOH	0.2	1.69	0.9	0.79	[4]
NC@Co-NGC DSNCs	0.1M KOH	0.4	1.64	0.82	0.82	[5]
$ZnCo_2O_4$/N-CNT	0.1M KOH	0.2	1.66	0.87	0.79	[6]
Co@Co_3O_4/NC-1	0.1M KOH	N/A	1.65	0.8	0.85	[7]
NiCo2S4/N-CNT	0.1M KOH	0.248	1.60	0.80	0.80	[8]
$Co_{1-x}S$/Graphene	0.1M KOH	0.1	1.58	0.755	0.825	[9]
CoO_x NPs/BNG	0.1M KOH	N/A	1.52	0.8	0.72	[10]
S,N-Fe/N/C-CNT	0.1M KOH	N/A	1.60	0.85	0.75	[11]
S-GNS/$NiCoS_4$	0.1M KOH	0.42	1.57	0.88	0.69	[12]
Ni_3FeN/CoN-CNF	0.1M KOH	N/A	1.50	0.80	0.7	[13]
CoNCF-1000-80	0.1M KOH	0.2	1.66	0.83	0.83	[14]
$CoNiO_2$-8	1.0 M KOH	0.2	1.499	0.837	0.662	[15]
CoO/r-NLG	1.0 M KOH	0.4	1.525	0.89	0.635	This work

Table S4. Comparison of the performances of Zn-air batteries with various bifunctional electrocatalysts.

Catalyst	Electrolyte	Specific capacity (mAh g_{zn}^{-1})	Energy density (Wh kg_{zn}^{-1})	Cycle condition (mA cm^{-2})	Ref.
NCNF	6.0 M KOH + 0.20 M ZnCl2	626	776	10	[16]
NCNF/CoxMn1-xO	6.0 M KOH + 0.20 M ZnCl2	581	695	7	[17]
Ag-Cu on Ni foam	6.0 M KOH + 0.20 M ZnCl2	572	641	20	[18]
NCNT/CoO-NiONiCo	6.0 M KOH + 0.20 M ZnCl2	594	713	7	[19]
CoZn-NC-700	6.0 M KOH + 0.10 M ZnCl2	578	694	10	[20]
Ni3Fe/N-C	6.0 M KOH + 0.10 M ZnCl2	528	634	10	[21]
CoNCF-1000-80	6.0 M KOH + 0.20 M Zn(Ac)2	650	797	10	[14]
BHPC-950	6.0 M KOH	797	963	20	[22]
CoO/r-NLG	6.0 M KOH + 0.20 M Zn(Ac)2	665.3	798.3	10	This work

Supplementary References

1 H. B. Yang, J. Miao, S.-F. Hung, J. Chen, H. B. Tao, X. Wang, L. Zhang, R. Chen, J. Gao, H. M. Chen, L. Dai and B. Liu, *Sci. Adv.*, 2016, **2**, e1501122–e1501122.

2 S. S. Shinde, C. H. Lee, A. Sami, D. H. Kim, S. U. Lee and J. H. Lee, *ACS Nano*, 2017, **11**, 347–357.

3 G. Li, X. Wang, J. Fu, J. Li, M. G. Park, Y. Zhang, G. Lui and Z. Chen, *Angew. Chemie - Int. Ed.*, 2016, **55**, 4977–4982.

4 T. Wang, Z. Kou, S. Mu, J. Liu, D. He, I. S. Amiinu, W. Meng, K. Zhou, Z. Luo, S. Chaemchuen and F. Verpoort, *Adv. Funct. Mater.*, 2018, **28**, 1705048.

5 S. Liu, Z. Wang, S. Zhou, F. Yu, M. Yu, C. Y. Chiang, W. Zhou, J. Zhao and J. Qiu, *Adv. Mater.*, 2017, **29**, 1700874.

6 Z. Q. Liu, H. Cheng, N. Li, T. Y. Ma and Y. Z. Su, *Adv. Mater.*, 2016, **28**, 3777–3784.

7 A. Aijaz, J. Masa, C. RÃ¶sler, W. Xia, P. Weide, A. J. R. Botz, R. A. Fischer, W. Schuhmann and M. Muhler, *Angew. Chemie - Int. Ed.*, 2016, **55**, 4087–4091.

8 X. Han, X. Wu, C. Zhong, Y. Deng, N. Zhao and W. Hu, *Nano Energy*, 2017, **31**, 541–550.

9 Y. Xu, Y. Hao, G. Zhang, X. Jin, L. Wang, Z. Lu and X. Sun, *Part. Part. Syst. Charact.*, 2016, **33**, 569–575.

10 Y. Tong, P. Chen, T. Zhou, K. Xu, W. Chu, C. Wu and Y. Xie, *Angew. Chemie - Int. Ed.*, 2017, **56**, 7121–7125.

11 P. Chen, T. Zhou, L. Xing, K. Xu, Y. Tong, H. Xie, L. Zhang, W. Yan, W. Chu, C. Wu and Y. Xie, *Angew. Chemie - Int. Ed.*, 2017, **56**, 610–614.

12 W. Liu, J. Zhang, Z. Bai, G. Jiang, M. Li, K. Feng, L. Yang, Y. Ding, T. Yu, Z. Chen and A. Yu, *Adv. Funct. Mater.*, 2018, **28**, 1706675.

13 Q. Wang, L. Shang, R. Shi, X. Zhang, G. I. N. Waterhouse, L. Z. Wu, C. H. Tung and T. Zhang, *Nano Energy*, 2017, **40**, 382–389.

14 H. Jiang, Y. Liu, W. Li and J. Li, *Small*, 2018, **14**, 1703739.

15 Y. Z. Jin, Z. Li, J. Q. Wang, R. Li, Z. Q. Li, H. Liu, J. Mao, C. K. Dong, J. Yang, S. Z. Qiao and X. W. Du, *Adv. Energy Mater.*, 2018, **8**, 1703469.

16 Q. Liu, Y. Wang, L. Dai and J. Yao, *Adv. Mater.*, 2016, **28**, 3000–3006.

17 X. Liu, M. Park, M. G. Kim, S. Gupta, X. Wang, G. Wu and J. Cho, *Nano Energy*, 2016, **20**, 315–325.

18 Y. Jin and F. Chen, *Electrochim. Acta*, 2015, **158**, 437–445.

19 X. Liu, M. Park, M. G. Kim, S. Gupta, G. Wu and J. Cho, *Angew. Chemie - Int. Ed.*, 2015, **54**, 9654–9658.

20 B. Chen, X. He, F. Yin, H. Wang, D. J. Liu, R. Shi, J. Chen and H. Yin, *Adv. Funct. Mater.*, 2017, **27**, 1700795.

21 G. Fu, Z. Cui, Y. Chen, Y. Li, Y. Tang and J. B. Goodenough, *Adv. Energy Mater.*, 2017, **7**, 1601172.

22 M. Yang, X. Hu, Z. Fang, L. Sun, Z. Yuan, S. Wang, W. Hong, X. Chen and D. Yu, *Adv. Funct. Mater.*, 2017, **27**, 1701971.